Geophysical Journal International

Geophys. J. Int. (2015) **201,** 1657–1665 doi: 10.1093/gji/ggv103
GJI Seismology

Inner core structure behind the PKP core phase triplication

Nienke A. Blom,[1] Arwen Deuss,[1] Hanneke Paulssen[1] and Lauren Waszek[2]

[1]*Department of Earth Sciences, Universiteit Utrecht, Budapestlaan* 4, *NL-*3584 *CD Utrecht, The Netherlands. E-mail:* n.a.blom@uu.nl
[2]*Bullard Laboratories, Department of Earth Sciences, University of Cambridge, Cambridge* CB3 0EZ, *UK*

Accepted 2015 February 27. Received 2015 February 12; in original form 2014 March 12

SUMMARY

The structure of the Earth's inner core is not well known between depths of ∼100–200 km beneath the inner core boundary. This is a result of the PKP core phase triplication and the existence of strong precursors to PKP phases, which hinder the measurement of inner core compressional PKIKP waves at epicentral distances between roughly 143 and 148°. Consequently, interpretation of the detailed structure of deeper regions also remains difficult. To overcome these issues we stack seismograms in slowness and time, separating the PKP and PKIKP phases which arrive simultaneously but with different slowness. We apply this method to study the inner core's Western hemisphere beneath South and Central America using paths travelling in the quasi-polar direction between 140 and 150° epicentral distance, which enables us to measure PKiKP–PKIKP differential traveltimes up to greater epicentral distance than has previously been done. The resulting PKiKP–PKIKP differential traveltime residuals increase with epicentral distance, which indicates a marked increase in seismic velocity for polar paths at depths greater than 100 km compared to reference model AK135. Assuming a homogeneous outer core, these findings can be explained by either (i) inner core heterogeneity due to an increase in isotropic velocity or (ii) increase in anisotropy over the studied depth range. Although this study only samples a small region of the inner core and the current data cannot distinguish between the two alternatives, we prefer the latter interpretation in the light of previous work.

Key words: Core, outer core and inner core; Body waves; Seismic anisotropy.

1 INTRODUCTION

Given its remoteness and small size (less than 1 per cent of the Earth's volume), the inner core plays a surprisingly important role in the Earth's dynamics. Discovered less than a century ago (Lehmann 1936), it is still relatively unknown, although many enigmatic characteristics have come to light over the past few decades. It has been found to be anisotropic, with the axis of symmetry approximately along the Earth's rotation axis and rays in the polar direction travelling faster than those in the equatorial plane (e.g. Morelli *et al.* 1986; Woodhouse *et al.* 1986). More recently, it was discovered to have two seismically distinct hemispheres (Tanaka & Hamaguchi 1997) that are separated by sharp boundaries (Waszek *et al.* 2011). The quasi-Western hemisphere has a lower velocity and stronger anisotropy than the quasi-Eastern hemisphere (Creager 1999; Garcia & Souriau 2000; Niu & Wen 2001a; Deuss *et al.* 2010; Irving & Deuss 2011; Waszek & Deuss 2011; Lythgoe *et al.* 2014). Internally, the hemispheres are not homogeneous either, as both isotropic and anisotropic velocities are found to vary laterally and with depth (e.g. Creager 1997; Waszek & Deuss 2011; Tkalčić *et al.* 2013).

A variety of different mechanisms have been proposed to explain both the anisotropy and the existence of hemispheres, all depending on how the inner core interacts with the surrounding outer core and mantle. While some propose that the anisotropy is frozen into the inner core as it solidifies (Karato 1993; Bergman 1997), others suggest that it formed later on, as a result of thermal convection (Jeanloz & Wenk 1988), deformation due to anisotropic growth (Yoshida *et al.* 1996), or magnetic field stresses (Karato 1999; Buffett & Wenk 2001). Whatever the mechanism causing the anisotropy, it also has to be in accordance with the existence of structurally different hemispheres and any other lateral or depth variations inside the inner core (Deuss 2014; Tkalčić 2015). The hemispheres have been proposed to be due to either degree-one convection in the inner core, the so-called 'inner core translation' model (Alboussière *et al.* 2010; Monnereau *et al.* 2010), or alternatively they may be due to thermochemical outer core flow resulting in laterally varying solidification regimes at the inner core boundary (ICB; Aubert *et al.* 2008).

In order to be able to determine what processes govern this remotest part of the Earth, it is important to have an accurate idea of its structure. Progress has been made in recent years with the compilation of large sets of inner core body wave and normal mode data (e.g. Shearer & Toy 1991; Creager 1992; Song & Helmberger 1995; McSweeney *et al.* 1997; Creager 1999; Tkalčić *et al.* 2002; Wen & Niu 2002; Cao & Romanowicz 2004; Garcia *et al.* 2006; Cormier 2007; Irving & Deuss 2011; Waszek & Deuss 2011; Deuss *et al.* 2013; Lythgoe *et al.* 2014). While normal modes have the advantage of uniform coverage, they consist of long-period data and have limited depth resolution. Here, we are interested in a more detailed mapping of inner core structure and therefore short-period body waves are more suitable.

The upper parts of the inner core have been studied in relatively high detail. In the Western hemisphere, an isotropic layer of about 60 km in thickness seems to be present at the very top of the inner core (Shearer 1994; Song & Helmberger 1995), below which anisotropy increases to 2.8 per cent (Waszek & Deuss 2011). No such layer has been found in the Eastern hemisphere. The isotropic velocity of the upper Western hemisphere is lower than that of the Eastern hemisphere (Tanaka & Hamaguchi 1997; Creager 1999; Wen & Niu 2002; Waszek & Deuss 2011; Tanaka 2012), with internal variations detected as well (e.g. Stroujkova & Cormier 2004; Iritani *et al.* 2014). Anisotropy is however found to be larger in the Western hemisphere (∼3 per cent as opposed to 0.5–1 per cent in the Eastern hemisphere; Song & Helmberger 1995; Tanaka & Hamaguchi 1997; Niu & Wen 2002; Deuss *et al.* 2010; Irving & Deuss 2011). Much more uncertainty and variation are found concerning the seismic structures deeper in the inner core. Suggested values for anisotropy in the Western hemisphere vary widely from 2–4 per cent at depths of 100–200 km beneath the ICB (Creager 1999; Sun & Song 2008) to 8 per cent at depths >250 km (Song & Xu 2002; Lythgoe *et al.* 2014), while the Eastern hemisphere is generally found to be more isotropic (e.g. Sun & Song 2008; Irving & Deuss 2011).

This larger uncertainty at depth is partially due to an unfortunate geometry of ray paths and traveltimes. At epicentral distances of 130–143°, PKiKP and PKIKP are used to study the upper 100 km of the inner core. For epicentral distances larger than 148°, PKPbc, PKPab and PKIKP are used to study the inner core below ∼200 km depth [Fig. 1(a)]. Around 145°, however, these core phases all arrive very closely in time and their traveltime curves intersect [Fig. 1(b)]. The presence of the PKP caustic at the B point in the traveltime curve (which results in very large PKPbc amplitudes drowning out the other phases), the intersections of the traveltime curves and strong precursors to PKP at smaller epicentral distances together make it very difficult to recognize individual PKP phases in the seismogram around ∼143–148° so that there are almost no measurements [Fig. 1(c)]. As a result, the spherical shell at depths of ∼100–200 km below the ICB is difficult to image using direct seismic observation and, consequently, uncertainties at depth remain large.

In this study, we attempt to bridge the gap between 143 and 148° by stacking seismograms in slowness and time in order to separate the PKP core phases and measure PKiKP–PKIKP differential traveltimes. Our efforts focus on the Western hemisphere, which is strongly anisotropic in the upper part, but whose anisotropy in deeper regions is still a subject of discussion. Another reason for focusing on polar paths is that we expect PKIKP to arrive earlier, leading to a greater separation from the other PKP phases, thus making it a favourable setting to test our method.

We will first discuss our stacking and data processing method. Then, we will present PKiKP–PKIKP differential travel time measurements and finally we will interpret our results in terms of inner core velocity structure.

2 METHODS AND DATA

We study the inner core using PKIKP (also called PKPdf), a compressional seismic body wave which travels through the mantle, the outer core and the inner core (Fig. 1). As a reference phase we use PKiKP, which travels along nearly the same path but reflects off the ICB. The other PKP phases are PKPab and PKPbc, which travel through the mantle and the outer core only. Because the paths of PKIKP and PKiKP are so close together, heterogeneities in the mantle encountered along the way will affect both rays in nearly the same way so that no corrections for 3D mantle structure need to be applied. Likewise, a potential mislocation of the earthquake hypocentre will have almost the same effect on both phases. The differential traveltime between these two phases can therefore be

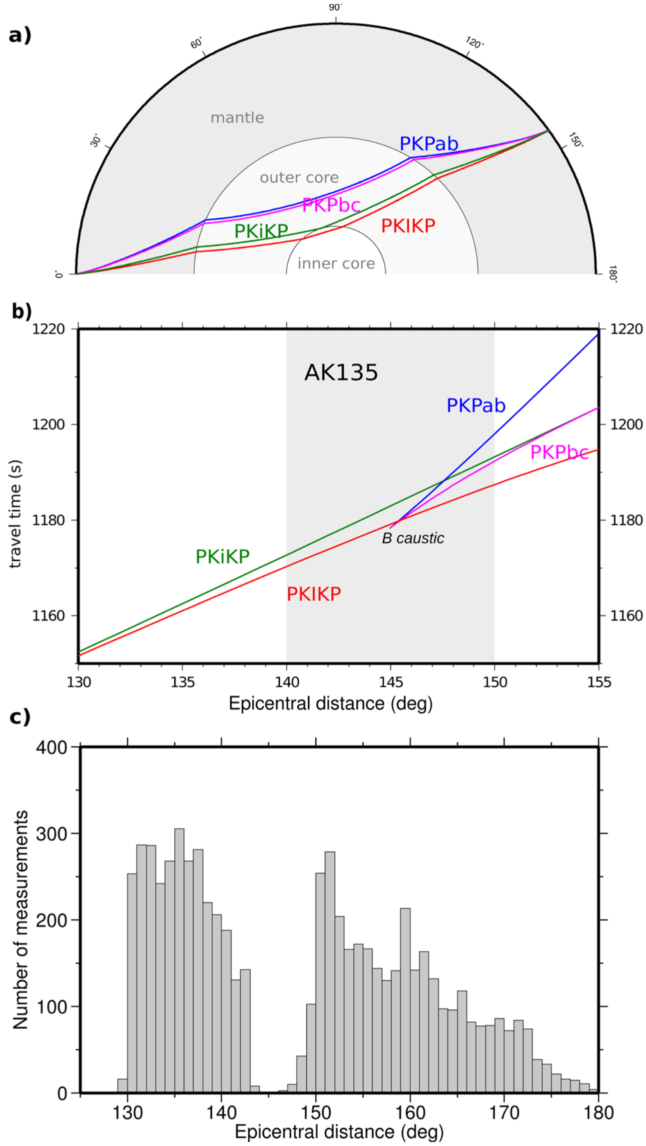

Figure 1. (a) Ray paths of the different compressional seismic phases that pass through the core. PKIKP (red) passes through the inner core, PKiKP (green) reflects off the inner core boundary, PKPbc (purple) travels through the deep outer core and PKPab (blue) passes through the shallower outer core. (b) Traveltime curves for the same phases at epicentral distances of 130–155°, calculated for AK135. The shaded area between 140 and 150° indicates the range of epicentral distances which has been ignored in previous studies, and the caustic at the B point is indicated. (c) Histogram showing the frequency of differential and absolute PKIKP measurements used in previous studies as a function of epicentral distance. A clear gap is visible at epicentral distances of ∼143–148°. The histogram was generated from data from Waszek & Deuss (2011), Irving & Deuss (2011) and Lythgoe *et al.* (2014).

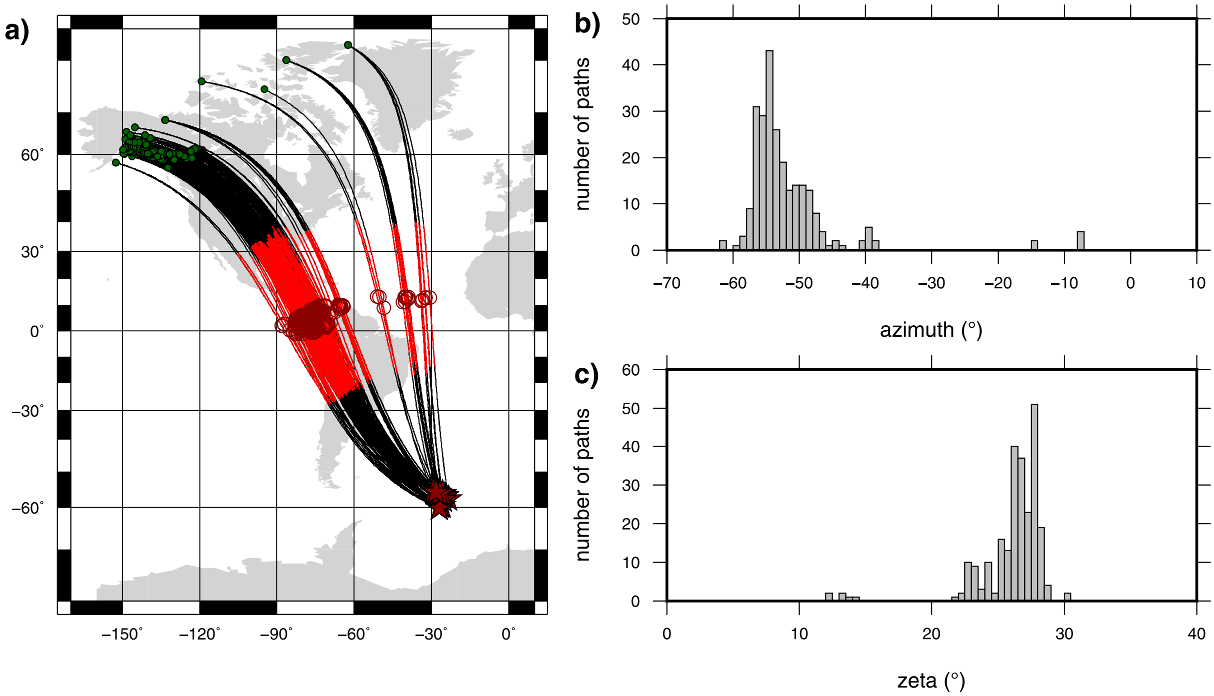

Figure 2. (a) Ray paths of all the seismograms used for the computation of the vespagrams between 140 and 150° epicentral distance. Dark red stars are the events (see Table 1), green dots the stations and the red part of the ray path is the portion which goes through the inner core, where the turning point is denoted with a dark red circle. (b) Histogram showing the range of ray-path azimuths of the used seismograms. Most of the rays leave the event with an azimuth of 60 to 40° W of N. (c) Histogram showing the range of ζ of the used seismograms. To a large extent, this is the mirror image of the range of azimuths because zeta is always a positive number and the used azimuths are all below zero. Because almost all rays turn very close to the equator, zeta is around half of the absolute value of the azimuth.

used to study the inner core because this is where the ray paths deviate: a difference between the observed PKiKP–PKIKP differential traveltime and a model prediction can be attributed to inner core structure. Studied as a function of epicentral distance, it gives information about the depth dependence of inner core seismic velocity. PKiKP–PKIKP has thus been used to study the upper 100 km of the inner core at epicentral distances of 130–143° (e.g. Niu & Wen 2001a; Wen & Niu 2002; Cao & Romanowicz 2004; Waszek & Deuss 2011).

As PKIKP and PKiKP cannot be distinguished individually from single seismograms between 143 and 147°, we combine the traces in stacks. For each event, we divide the data in bins of epicentral distance, stacking the traces from different stations for a large range of slownesses. The results are visualized in a plot called vespagram, which displays signal amplitude as a function of slowness p and traveltime t (Davies *et al.* 1971). This method has been used before to study core phases (Davies *et al.* 1971; Doornbos & Husebye 1972; Schlittenhardt 1996), and we apply it here to separate PKIKP and PKiKP from PKPab and PKPbc in the range where all these phases interfere. We employ the Phase Weighted Stack (PWS) technique (Schimmel & Paulssen 1997), where the sum of the seismograms is weighted by the coherency of their instantaneous phase.

We focus on polar paths in the Western hemisphere, whose traveltimes are known to be anomalous, while equatorial traveltimes are close to those predicted by globally averaged 1-D models (Creager 1999; Niu & Wen 2002; Irving & Deuss 2011). We define polar paths as paths where the angle ζ between the Earth's rotation axis and the direction of the ray path at its turning point is smaller than 35°. Events with magnitudes of $M_W > 5.5$ are selected based on locations yielding polar paths. High-quality recordings from South Sandwich Islands subduction events to stations mainly in North-West Canada and Alaska are abundant and are therefore suitable for our aims (see Fig. 2). All used events have magnitudes around $M_W = 6$ and at depths up to 200 km (see Table 1).

The gathered seismic traces are filtered between 0.5 and 2 Hz, and checked for quality. The traces for each event are then divided into bins of 5° epicentral distance: 140–145°, 142.5–147.5°, 145–150° and 150–155°, and stacked, where any bin containing fewer than four traces is discarded. The bins contain data from arrays and single stations, all for the same event, so that within a single bin, azimuths may vary by as much as 51° and ζ by as much as 13° (see also Table 1). The combination of different stations ensures that station specific biases are averaged out and a more robust result is obtained. The combination of multiple traces into a stack also helps reduce the scatter typical of individually interpreted waveforms, making it possible to achieve a more stable mean measure of differential traveltime. The traces are normalized and stacked with PWS at slownesses ranging between 0 and 5 s deg^{-1}. Within each bin, the median epicentral distance is used as the reference for the stack. This ensures that the differential traveltime is calculated at the distance where most of the data are found, and that the resulting vespagram does not become distorted as a result of unbalanced epicentral distance distribution within the bin.

We measure differential traveltimes from the vespagrams that are thus generated for each event and each bin. Traveltimes are hand-picked from phase onsets in the vespagrams. The slowness where a phase has the largest amplitude is selected as the slowness for that particular phase. Traveltimes are then compared to predictions from velocity model AK135 (Kennett *et al.* 1995), and differential traveltime residuals δt are calculated with

$$\delta t = (t_{\mathrm{PKiKP}} - t_{\mathrm{PKIKP}})_{\mathrm{data}} - (t_{\mathrm{PKiKP}} - t_{\mathrm{PKIKP}})_{\mathrm{model}}. \quad (1)$$

Table 1. Overview of differential traveltime data. Events are from the South Sandwich Islands region, recording stations are mostly located in Alaska and Northwest Canada. Δ_{ref} is the reference epicentral distance in the stack and $t_{\mathrm{ref}} - t_{\mathrm{I}} = (t_{\mathrm{PKiKP}} - t_{\mathrm{PKIKP}})_{\mathrm{data}}$ for the bins 140–145°, 142.5–147.5° and 145–150° (top three sections of the table) and $t_{\mathrm{ref}} - t_{\mathrm{I}} = (t_{\mathrm{PKPbc}} - t_{\mathrm{PKIKP}})_{\mathrm{data}}$ for the bin 150–155° (bottom section). Data from overlapping bins have been omitted.

Event date & time (UTC)	M_{W}	Depth (km)	Δ_{ref} (°)	ζ range (°)	n_{seis}	$t_{\mathrm{ref}} - t_{\mathrm{I}}$ (s)
2004-09-06 14:17:19.3	5.8	10.0	142.33	26.11–27.62	8	4.4
2004-09-11 21:53:38.3	6.1	63.9	142.26	13.25–26.79	19	5.0
2004-10-08 15:28:39.2	5.9	101.5	143.60	26.21–27.48	5	4.5
2004-10-26 22:53:07.8	6.2	10.0	143.13	24.12–27.29	9	5.4
2005-05-18 09:10:53.6	6.0	102.2	143.54	26.36–27.53	4	5.1
2005-06-12 19:26:24.8	6.0	94.1	142.78	26.39–27.30	4	4.2
2005-07-25 19:45:16.0	5.5	84.8	142.94	24.92–27.47	5	4.7
2005-08-04 12:11:21.3	5.6	45.9	142.86	21.63–25.96	20	4.3
2004-11-07 02:41:41.0	5.8	38.6	145.64	23.15–27.75	6	5.7
2006-05-29 05:20:48.4	5.7	124.4	145.50	12.42–25.60	4	6.6
2004-09-06 14:17:19.3	5.8	10.0	148.83	25.71–30.19	18	8.5
2005-08-04 12:11:21.3	5.6	45.9	145.81	21.63–25.96	7	6.0
2005-09-09 19:55:21.8	5.6	142.8	148.33	23.05–28.55	11	8.1
2008-04-14 09:45:19.7	6.0	140.2	149.36	23.04–28.58	29	8.4
2010-12-08 05:24:35.2	6.3	29.4	147.73	23.15–28.01	26	7.7
2011-08-21 12:38:53.7	5.6	130.4	147.87	22.92–27.93	26	8.2
2011-09-03 04:48:57.3	6.4	84.0	147.45	22.99–27.84	21	8.5
2011-12-11 09:54:55.2	6.2	116.0	147.58	23.03–28.53	32	8.1
2004-09-11 21:53:38.3	6.1	63.9	152.54	24.31–34.70	25	10.0
2004-10-08 15:28:39.2	5.9	101.5	151.40	25.29–29.88	17	9.5
2005-05-18 09:10:53.6	6.0	102.2	151.33	23.88–33.38	17	9.0
2005-06-12 19:26:24.8	6.0	94.1	151.16	23.92–33.46	25	10.2
2005-08-04 12:11:21.3	5.6	45.9	152.91	23.90–31.75	11	11.5
2011-03-06 14:32:36.0	6.5	87.7	151.92	25.09–33.40	34	10.1
2011-09-03 04:48:57.0	6.4	84.0	152.00	24.65–33.36	32	10.6
2011-12-11 09:54:55.2	6.2	116.0	150.84	25.41–33.71	28	8.4

Model traveltimes are calculated using TauP (Crotwell *et al.* 1999) and residuals are initially calculated with respect to AK135. Unless stated otherwise, all depths mentioned in this paper have been calculated for AK135. For comparison, we also calculate synthetic seismograms with the WKBJ modelling method (Chapman 1978) for model AK135, using the same source parameters and station locations as the real data and processed in the same way.

3 OBSERVATIONS

Fig. 3 shows the seismograms from a South Sandwich Islands event on 2004 September 11 (21:53:38.3, $M_{\mathrm{W}} = 6.1$, depth = 63.9 km) as a function of epicentral distance. Because of the near-simultaneous arrivals, it is impossible to separate PKIKP and PKiKP from PKPab and PKPbc around 145° in single seismograms. In addition, the PKP precursors, which become increasingly pronounced towards 145°, obscure PKIKP and PKiKP arrivals at smaller epicentral distances. Our stacking efforts will be focused on this epicentral distance range. Examples of the corresponding vespagrams are plotted in Fig. 4.

As a proof of concept, we first compare vespagrams from real and synthetic WKBJ seismograms between 150 and 155°, a range where the PKP phases are clearly separated and PKIKP and PKPbc can be picked easily from individual seismograms (see Fig. 3). There is good correspondence between synthetic and real data vespagrams [Figs 4(a) and (b)] and also between the vespagram arrivals and TauP predictions (Crotwell *et al.* 1999; plotted as pluses in Fig. 4). The only difference is that in the real data vespagram, PKIKP arrives considerably earlier and at smaller slowness than predicted by AK135. As a result, measured PKPbc–PKIKP differential traveltimes (Table 1) are larger than predicted. We also see additional, smaller arrivals, but the main phases can be identified unambiguously.

We now apply the same stacking technique to the bins of 140–145°, 142.5–147.5° and 145–150°, which cover the whole region in which the PKP phases are difficult to pick from individual seismograms. In the resulting vespagrams, both from real and synthetic seismograms [see Figs 4(c)–(f)], PKIKP and PKiKP are visible as clearly identifiable, separate arrivals. This is important, firstly, because it means that the effect of the PKP triplication can be circumvented by stacking, allowing the phases to be separated. Secondly, PKiKP differential travel time remains detectable up to 150°, which enables us to measure PKiKP–PKIKP differential traveltimes up to greater epicentral distance than has previously been done.

PKIKP and PKiKP have opposite polarities in both observed and synthetic vespagrams, a result of PKiKP being reflected, while PKIKP is transmitted at the ICB. In the real data vespagrams [Figs 4(d) and (f)], we also see that the PKIKP waveform becomes wider and of smaller amplitude with increasing epicentral distance. This is probably due to a longer path in the inner core, where attenuation is larger (Li & Cormier 2002; Yu & Wen 2006) and where attenuation anisotropy may result in anomalously low amplitudes for quasi-polar paths (Souriau & Romanowicz 1996; Creager 1999).

We then measure differential traveltimes for PKiKP and PKIKP from their phase onsets in constant slowness cross-section at the maximum amplitude of each phase. Generally, we see that PKIKP tends to arrive earlier and with smaller slowness than predicted for

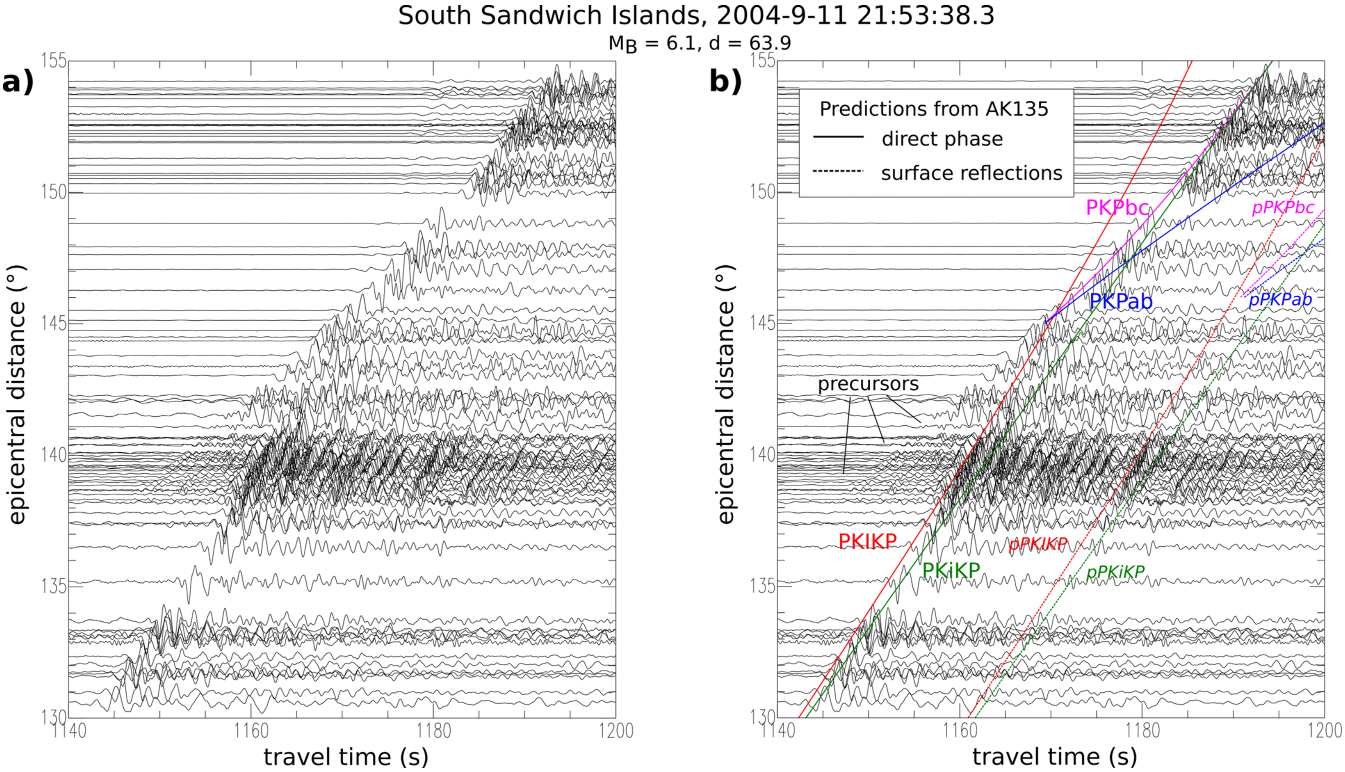

Figure 3. (a) Seismograms for PKIKP signals travelling in the Western hemisphere in the polar direction ($\zeta < 35°$), filtered around 1 Hz. (b) The same as (a), but with predictions for the arrival times are shown as solid lines (direct phases) and dotted lines (surface reflections), calculated for model AK135 and using the same colours as in Fig. 1.

model AK135; PKiKP–PKIKP differential traveltime residuals are thus larger than predicted by AK135 and in addition increase with epicentral distance. This agrees with what we observed at 150–155° for PKPbc–PKIKP.

Apart from the main arrivals, additional smaller phases are visible in the observed data vespagrams. The most notable among these are a line of distinct arrivals visible in the bin for 140–145° [Fig. 4(f)], starting from the PKIKP arrival time and slowness, and then continuing to larger slownesses and earlier arrival times. These are PKP precursors (Doornbos & Husebye 1972; Hedlin *et al.* 1997; Niu & Wen 2001b; Margerin & Nolet 2003; Cao & Romanowicz 2007; Thomas *et al.* 2009) which are also clearly visible in the individual seismograms of Fig. 3 in the same epicentral distance range. Even though in single seismograms the precursors make it difficult to distinguish individual PKP peaks, the vespagrams allow us to successfully separate PKIKP and PKiKP from the PKP precursors and measure differential traveltimes. In some vespagrams (not shown here), depth phases can also be distinguished, but these do not interfere with the direct core phases. Thus, the use of vespagrams also helps us in separating the depth phases from the direct phases.

We investigated a total of 30 events and found that 16 of these produced vespagrams of sufficient quality to enable us to measure differential traveltimes $(t_{\mathrm{PKiKP}} - t_{\mathrm{PKIKP}})_{\mathrm{data}}$. This resulted in nine measurements for the 140–145° bin, eight at 145–150° and four at 142.5–147.5°. Table 1 shows the measurement details for each (non-overlapping) event and bin. The relatively high rejection rate is a result of quality requirements—both PKIKP and PKiKP must be clearly distinguishable in the vespagram. In addition, some bins did not contain enough seismograms to allow for stacking. The PKiKP–PKIKP differential travel time residuals δt (eq. 1) are calculated for model AK135 and shown in Fig. 5(a) for all bins. Only residuals from non-overlapping data bins are included and all our measurements are for polar paths. We find that residuals for model AK135 become larger with increasing epicentral distance, which corresponds to waves travelling deeper in the inner core. This trend is visible across the different bins, and it means that for these paths a larger increase in seismic velocity with depth than AK135 is needed to explain our observations.

The ray paths of PKIKP and PKiKP are very close together, so it is unlikely that mantle structure has an effect on their differential traveltime. However, some studies have found strong effects of mantle structure on PKPab–PKIKP and PKPbc–PKIKP differential traveltimes (Bréger *et al.* 1999, 2000; Tkalčić *et al.* 2002), whose paths are farther apart. To further assess to what extent the path separation may play a role, we analyse $(t_{\mathrm{PKPab}} - t_{\mathrm{PKPbc}})_{\mathrm{data}}$ measurements at 150–155°. Even with a much larger path separation, PKPab–PKPbc residuals obtained from these measurements average at 0.2 s with a scatter of 0.8 s. This is significantly smaller than our measured PKPbc–PKIKP residuals in the same distance range, which average at 3.1 s with a scatter of 1.3 s, in accordance with previous studies (e.g. Morelli *et al.* 1986; Shearer 1994; Creager 1999; Irving & Deuss 2011). Moreover, the systematic trend of increasing differential traveltime with epicentral distance over different sources that we see in our results makes it unlikely that a mantle heterogeneity is its cause.

4 INTERPRETATION

We compare our measured differential traveltimes (Table 1) to predictions for various models. Table 2 sums up the residual sums of squares (RSS) for the various models, which is an indication for the

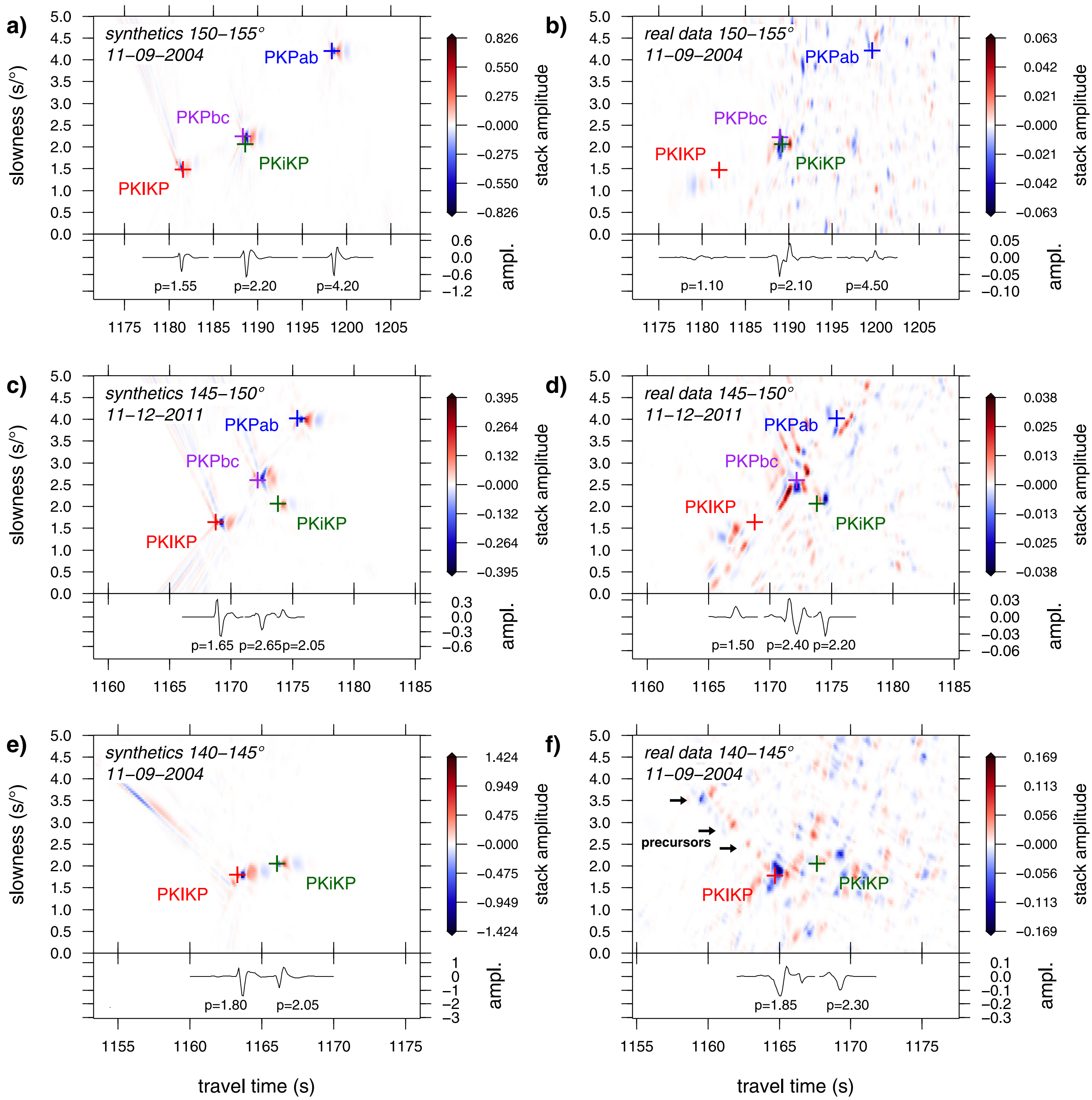

Figure 4. Vespagrams produced using the Phase Weighted Stacking technique with $\nu = 3$ [see Schimmel & Paulssen (1997)] for South Sandwich Islands events of 2004 September 11 and 2011 December 11. (a, b) Stacks of the epicentral distance bin 150–155°; (c, d) bin 145–150°; (e, f) bin 140–145°. Vespagrams in the left column (a, c, e) are computed from synthetic data, those on the right (b, d, f) from the real observed data. Model predictions for the arrival time and slowness of the direct phases and surface reflections for model A135 are plotted as pluses. The bottom panel in each subplot shows cross sections through the vespagrams at the appropriate slowness for the PKP phases. These cross sections are used to measure differential traveltimes.

goodness of fit. The positive residuals increasing with epicentral distance that were found for model AK135 [Fig. 5(a)] produce a very large RSS of ∼112 s^2. To reduce the misfit, an increase in seismic velocity with depth appears necessary.

Waszek & Deuss (2011) constructed inner core velocity models for the upper ∼100 km of the inner core based on PKiKP–PKIKP measurements up to ∼143°. Beneath 60 km beneath the ICB, they find 2.8 per cent anisotropy for the Western inner core, the result of a 0.3 km s^{-1} velocity increase in their model for polar paths. However, this velocity increase (attributed to anisotropy) is not sufficient to remove the positive differential traveltime residuals that we measure, even if the larger velocities are extended to depths beyond 100 km beneath the ICB (model WDpolW-ext in Fig. 5).

To investigate the constraints that our data put on velocity structure below 100 km, we perform a model space search minimizing the RSS for the PKiKP–PKIKP measurements in a least-squares sense. A gradual increase in velocity is imposed, where the starting depth of the velocity increase and the velocity gradient are taken as free parameters. The 'best-fit' model NpolW reduces the RSS to 3.07 s^2, and we also obtain a range of models with

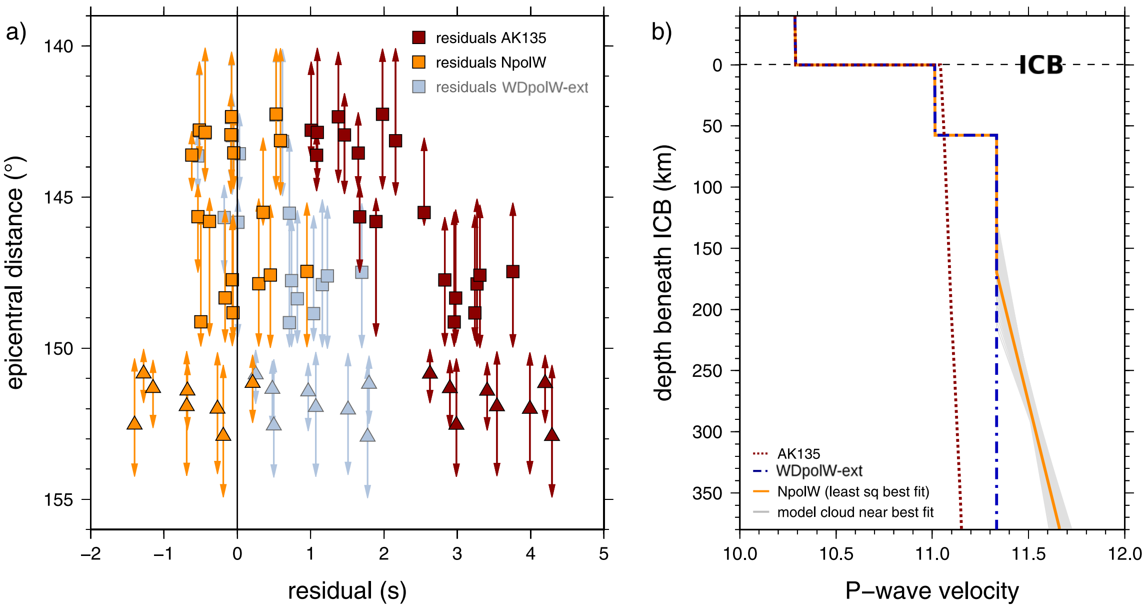

Figure 5. (a) Differential traveltime residuals of PKiKP–PKIKP for the data in the bins 140–145°, 142.5–147.5° and 145–150° (squares), and of PKPbc–PKIKP for the bin 150–155 (triangles). The residuals have been calculated with eq. (1) for models AK135 (red), the 'best-fit' model NpolW (yellow) and WDpolW-ext (light blue). Residuals are plotted at the reference epicentral distance of the stack, and the vertical arrows indicate the actual width of the epicentral distance bin, which is variable according to the exact spread of stations that were available. (b) Velocity models used in this study. Model NpolW (yellow) is the least-squares minimum RSS model generated using PKiKP–PKIKP differential traveltimes at epicentral distances of 140–150° obtained in this study (RSS = 3.07). The models plotted in grey around it have a similar fit to the data (RSS < 4) and show the trade-off between starting depth and gradient of the velocity increase.

Table 2. Residual sum of squares (RSS) for the different models tested in this study.

Model name	RSS (s^2)
AK135	111.74
WDpolW-106	64.05
WDpolW-ext	13.36
NpolW	3.07

similar fit [Fig. 5(b)]. Although there is a significant trade-off between starting depth and velocity gradient, it is evident that our polar path data require an increase in velocity with depth (simultaneously resulting in deeper penetration of the rays into the inner core). This is in line with results of previous PKPbc–PKIKP studies, which also show an increase in polar velocity with depth (McSweeney *et al.* 1997; Niu & Wen 2002; Sun & Song 2008; Irving & Deuss 2011). It also agrees with the PKPbc–PKIKP differential traveltimes that we measured ourselves from vespagrams at 150–155°, although the 'best-fit' model slightly seems to overshoot the velocity gradient. This may be a result of both the trade-off, the limited amount of data and possibly the fact that PKPbc–PKIKP paths are more widely separated. The most important message from our polar data is that an increase in velocity with depth is needed to explain them.

We also investigate our data as a function of ζ (Fig. 6), but find that our polar data only have a limited range of ζ, preventing us from determining the velocity in the quasi-equatorial direction.

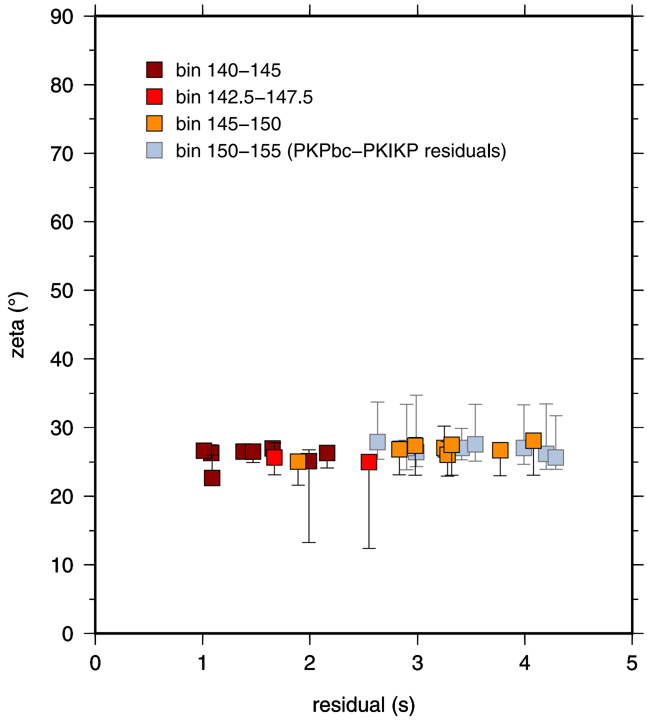

Figure 6. Differential traveltimes residuals of PKiKP–PKIKP with respect to model AK135. The residuals are the same as in Fig. 5 but as a function of ζ. Residuals are plotted at the median ζ of the bin, and the vertical bars indicate the variation of ζ within the bin. The median ζ is ~25–27° for all bins.

5 DISCUSSION

To our knowledge, this is the first study to measure PKiKP–PKIKP residuals at distances beyond 143° and up to 150°. The data—polar ray paths travelling through the Western inner core beneath Central/South America—require a velocity increase with depth in the inner core for at least the region sampled. We did not find any events that would allow us to make observations of equatorial paths in the region, thus preventing us from investigating the variation of velocity as a function of ζ.

The increase in velocity with depth for polar paths in this region is either due to end-member hypotheses (i) an increase in isotropic velocity or (ii) an increase in inner core anisotropy. An increase in isotropic velocity requires strong inner core heterogeneity, because the equatorial velocity would be increasing to values much larger than observed at other depths or laterally in the inner core for either equatorial or isotropic velocity variations (e.g. Sun & Song 2008; Irving & Deuss 2011). Without observations of equatorial paths in the same region it cannot be proven that anisotropy is the cause of the observed trend. However, we prefer to interpret our results as being due to an increase in anisotropy with depth for a number of reasons. The most important one is that the traveltimes for our global paths deviate so strongly from globally averaged models, which are essentially equatorial models. At the epicentral distances we are interested in (140–150°), there are 18 times as many conceivable equatorial paths as polar paths. Thus, global reference models like AK135 are effectively an equatorial average, and therefore a clear deviation from these traveltimes in polar paths is likely to be a result of anisotropy. Previous studies for shallower and deeper depths in the same region also find that polar paths yield anomalous traveltimes while equatorial traveltimes are close to those predicted by globally averaged 1-D models (Creager 1999; Niu & Wen 2002; Irving & Deuss 2011). In addition, normal modes indicate generally strong anisotropy in the inner core's Western hemisphere (e.g. Deuss *et al.* 2010). In our opinion, a smooth continuation of anisotropy, instead of a thin heterogeneous layer with a large increase in both equatorial and polar velocity, provides the most logical explanation.

An increase in anisotropy most likely means that the process responsible for the anisotropy is of a gradual or constant nature. One type of process that would fit our observations is a post-solidification process which acts on the whole of the inner core, for example, crystal alignment due to deformation because of thermal convection (Jeanloz & Wenk 1988), because of preferential growth in the equatorial region (Yoshida *et al.* 1996), or due to magnetic field stress (Karato 1999; Buffett & Wenk 2001). Deeper layers, which have been solid for a longer time, would then be more anisotropic. A heterogeneous increase in isotropic velocity, leading to locally anomalously fast equatorial and polar paths, would be more difficult to explain.

So far, we have only studied polar paths in the Western hemisphere. With the displacement of USArray to Alaska and increasing numbers of stations that come available in general, it will become possible to extend upon this data set. Adding equatorial paths and data for the Eastern hemisphere will be the subject of a further study, where velocity variations can be studied fully as a function of ζ in the depth range of 100–200 km in the upper part of the inner core. This will allow us to unambiguously distinguish between either an increase in isotropic or anisotropic velocity variations with depth.

6 CONCLUSION

We have shown that the combination of vespagrams with the PWS technique is a powerful tool to differentiate between simultaneously arriving, interfering phases. Smaller amplitude core phases such as PKiKP (which in single seismograms are hidden in the coda of the bigger PKPbc and PKPab phases) can be distinguished from PKIKP and its precursors, which have a clearly defined, separate signal. As a result, we have been able to bridge the gap in PKIKP measurements which existed between 143 and 148° and measured PKiKP–PKIKP differential traveltimes up to 150° epicentral distance.

Our new data set consists of quasi-polar paths, sampling a region of the Western hemisphere of the Earth's inner core beneath Central/South America at depths of 100–200 km below the ICB. Although there is a significant trade-off between starting depth of the velocity increase and its magnitude, the polar data require a larger increase in velocity with depth than AK135 in the inner core's Western hemisphere. The increase in velocity can either be due to an increase in isotropic velocity or anisotropic velocity. Without any observations of equatorial paths in the same region we cannot distinguish between these two alternatives, though we prefer an increase in anisotropic velocity given the context of previous work. Such an increase in anisotropy would support a post-solidification process as a cause of anisotropy in the inner core.

These results are also important for studies of the deeper inner core, as even a thin layer influences deeper traveltimes in a significant way. Because the shallower layers can now be accounted for more accurately, this will increase our understanding of the inner core as a whole.

ACKNOWLEDGEMENTS

We thank the editors, Vernon Cormier, and two other anonymous reviewers for their thorough reading of our paper and comments that helped improve the manuscript. Earthquake data have been collected from the Incorporated Research Institutions for Seismology (IRIS) Data Management Center (DMC) and the Canadian National Seismograph Network. The figures have been produced using GMT software (Wessel & Smith 1991, 1998). NB was funded by an EC Erasmus placement scholarship and is currently funded by the Dutch NWO VIDI grant number 864.11.008. AD is funded by the European Research Council under the European Community's Seventh Framework Programme (FP7/2007–2013)/ERC grant scheme number 204995 and by a Philip Leverhulme Prize. Part of NB's research was also supported by this grant. LW is funded by a research fellowship from Homerton College, University of Cambridge. We thank Jessica Irving and Karen Lythgoe for letting us use their data in our Fig. 1(c).

REFERENCES

Alboussière, T., Deguen, R. & Melzani, M., 2010. Melting-induced stratification above the Earth's inner core due to convective translation, *Nature,* **466,** 744–747.

Aubert, J., Amit, H., Hulot, G. & Olson, P., 2008. Thermochemical flows couple the Earth's inner core growth to mantle heterogeneity, *Nature,* **454,** 758–762.

Bergman, M.I., 1997. Measurements of electric anisotropy due to solidification texturing and the implications for the Earth's inner core, *Nature,* **389**(6646), 60–63.

Bréger, L., Romanowicz, B. & Tkalčić, H., 1999. PKP(BC-DF) travel time residuals and short scale heterogeneity in the deep Earth, *Geophys. Res. Lett.,* **26**(20), 3169–3172.

Bréger, L., Tkalčić, H. & Romanowicz, B., 2000. The effect of D′′ on PKP(AB-DF) travel time residuals and possible implications for inner core structure, *Earth planet. Sci. Lett.,* **175**(1), 133–143.

Buffett, B. & Wenk, H.-R., 2001. Texturing of the Earth's inner core by Maxwell stresses, *Nature,* **413**(6851), 60–63.

Cao, A. & Romanowicz, B., 2004. Hemispherical transition of seismic attenuation at the top of the Earth's inner core, *Earth planet. Sci. Lett.,* **228**(3), 243–253.

Cao, A. & Romanowicz, B., 2007. Locating scatterers in the mantle using array analysis of PKP precursors from an earthquake doublet, *Earth planet. Sci. Lett.,* **255**(1), 22–31.

Chapman, C.H., 1978. A new method for computing synthetic seismograms, *Geophys. J. R. astr. Soc.,* **54**(3), 481–518.

Cormier, V.F., 2007. Texture of the uppermost inner core from forward-and back-scattered seismic waves, *Earth planet. Sci. Lett.,* **258**(3), 442–453.

Creager, K.C., 1992. Anisotropy of the inner core from differential travel times of the phases PKP and PKIKP, *Nature,* **356**(6367), 309–314.

Creager, K.C., 1997. Inner core rotation rate from small-scale heterogeneity and time-varying travel times, *Science,* **278**(5341), 1284–1288.

Creager, K.C., 1999. Large-scale variations in inner core anisotropy, *J. geophys. Res.: Solid Earth (1978–2012),* **104**(B10), 23127–23139.

Crotwell, H.P., Owens, T.J. & Ritsema, J., 1999. The TauP toolkit: flexible seismic travel-time and ray-path utilities, *Seism. Res. Lett.,* **70**(2), 154–160.

Davies, D., Kelly, E. & Filson, J., 1971. Vespa process for analysis of seismic signals, *Nature,* **232,** 8–13.

Deuss, A., 2014. Heterogeneity and anisotropy of the Earth's inner core, *Annu. Rev. Earth. Planet. Sci.,* **42,** 103–126.

Deuss, A., Irving, J.C. & Woodhouse, J.H., 2010. Regional variation of inner core anisotropy from seismic normal mode observations, *Science,* **328**(5981), 1018–1020.

Deuss, A., Ritsema, J. & van Heijst, H., 2013. A new catalogue of normal-mode splitting function measurements up to 10 mHz, *Geophys. J. Int.,* **193**(2), 920–937.

Doornbos, D. & Husebye, E., 1972. Array analysis of PKP phases and their precursors, *Phys. Earth planet. Inter.,* **5,** 387–399.

Garcia, R. & Souriau, A., 2000. Inner core anisotropy and heterogeneity level, *Geophys. Res. Lett.,* **27**(19), 3121–3124.

Garcia, R., Tkalčić, H. & Chevrot, S., 2006. A new global PKP data set to study Earth's core and deep mantle, *Phys. Earth planet. Inter.,* **159**(1), 15–31.

Hedlin, M.A., Shearer, P.M. & Earle, P.S., 1997. Seismic evidence for small-scale heterogeneity throughout the Earth's mantle, *Nature,* **387**(6629), 145–150.

Iritani, R., Takeuchi, N. & Kawakatsu, H., 2014. Intricate heterogeneous structures of the top 300 km of the Earth's inner core inferred from global array data: I. regional 1D attenuation and velocity profiles, *Phys. Earth planet. Inter.,* **230,** 15–27.

Irving, J. & Deuss, A., 2011. Hemispherical structure in inner core velocity anisotropy, *J. geophys. Res.: Solid Earth (1978–2012),* **116**(B4), doi:10.1029/2010JB007942.

Jeanloz, R. & Wenk, H.-R., 1988. Convection and anisotropy of the inner core, *Geophys. Res. Lett.,* **15**(1), 72–75.

Karato, S.-i., 1993. Inner core anisotropy due to the magnetic field – induced preferred orientation of iron, *Science,* **262**(5140), 1708–1711.

Karato, S.-i., 1999. Seismic anisotropy of the Earth's inner core resulting from flow induced by Maxwell stresses, *Nature,* **402**(6764), 871–873.

Kennett, B., Engdahl, E. & Buland, R., 1995. Constraints on seismic velocities in the Earth from traveltimes, *Geophys. J. Int.,* **122**(1), 108–124.

Lehmann, I., 1936. P′, *Bur. Cent. Seismol. Int. Trav. Sci.,* **A14,** 87–115.

Li, X. & Cormier, V.F., 2002. Frequency-dependent seismic attenuation in the inner core, 1. A viscoelastic interpretation, *J. geophys. Res.,* **107**(B12), 2361, doi:10.1029/2002JB001795.

Lythgoe, K., Deuss, A., Rudge, J. & Neufeld, J., 2014. Earth's inner core: Innermost inner core or hemispherical variations?, *Earth planet. Sci. Lett.,* **385,** 181–189.

Margerin, L. & Nolet, G., 2003. Multiple scattering of high-frequency seismic waves in the deep Earth: PKP precursor analysis and inversion for mantle granularity, *J. geophys. Res.,* **108**(B11), 2514, doi:10.1029/2003JB002455.

McSweeney, T.J., Creager, K.C. & Merrill, R.T., 1997. Depth extent of inner-core seismic anisotropy and implications for geomagnetism, *Phys. Earth planet. Inter.,* **101**(1), 131–156.

Monnereau, M., Calvet, M., Margerin, L. & Souriau, A., 2010. Lopsided growth of Earth's inner core, *Science,* **328,** 1014–1017.

Morelli, A., Dziewonski, A.M. & Woodhouse, J.H., 1986. Anisotropy of the inner core inferred from PKIKP travel times, *Geophys. Res. Lett.,* **13**(13), 1545–1548.

Niu, F. & Wen, L., 2001a. Hemispherical variations in seismic velocity at the top of the Earth's inner core, *Nature,* **410**(6832), 1081–1084.

Niu, F. & Wen, L., 2001b. Strong seismic scatterers near the core-mantle boundary west of Mexico, *Geophys. Res. Lett.,* **28**(18), 3557–3560.

Niu, F. & Wen, L., 2002. Seismic anisotropy in the top 400 km of the inner core beneath the "eastern hemisphere, *Geophys. Res. Lett.,* **29**(12), 53–1.

Schimmel, M. & Paulssen, H., 1997. Noise reduction and detection of weak, coherent signals through phase-weighted stacks, *Geophys. J. Int.,* **130**(2), 497–505.

Schlittenhardt, J., 1996. Array analysis of core-phase caustic signals from underground nuclear explosions: discrimination of closely spaced explosions, *Bull. seism. Soc. Am.,* **86**(1A), 159–171.

Shearer, P.M., 1994. Constraints on inner core anisotropy from PKP (DF) travel times, *J. geophys. Res.: Solid Earth (1978–2012),* **99**(B10), 19 647–19 659.

Shearer, P.M. & Toy, K.M., 1991. PKP(BC) versus PKP(DF) differential travel times and aspherical structure in the Earth's inner core, *J. geophys. Res.: Solid Earth (1978–2012),* **96**(B2), 2233–2247.

Song, X. & Helmberger, D.V., 1995. Depth dependence of anisotropy of Earth's inner core, *J. geophys. Res.: Solid Earth (1978–2012),* **100**(B6), 9805–9816.

Song, X. & Xu, X., 2002. Inner core transition zone and anomalous PKP(DF) waveforms from polar paths, *Geophys. Res. Lett.,* **29**(4), 1042.

Souriau, A. & Romanowicz, B., 1996. Anisotropy in inner core attenuation: a new type of data to constrain the nature of the solid core, *Geophys. Res. Lett.,* **23**(1), 1–4.

Stroujkova, A. & Cormier, V.F., 2004. Regional variations in the uppermost 100 km of the Earth's inner core, *J. geophys. Res.: Solid Earth (1978–2012),* **109**(B10), doi:10.1029/2004JB002976.

Sun, X. & Song, X., 2008. Tomographic inversion for three-dimensional anisotropy of Earth's inner core, *Phys. Earth planet. Inter.,* **167**(1), 53–70.

Tanaka, S., 2012. Depth extent of hemispherical inner core from PKP(DF) and PKP(Cdiff) for equatorial paths, *Phys. Earth planet. Inter.,* **210,** 50–62.

Tanaka, S. & Hamaguchi, H., 1997. Degree one heterogeneity and hemispherical variation of anisotropy in the inner core from PKP(BC)-PKP(DF) times, *J. geophys. Res.: Solid Earth,* **102**(B2), 2925–2938.

Thomas, C. *et al.*, 2009. Probing two low-velocity regions with PKP b-caustic amplitudes and scattering, *Geophys. J. Int.,* **178**(1), 503–512.

Tkalčić, H., 2015. Complex inner core of the Earth: the last frontier of global seismology, *Rev. Geophys.,* doi:10.1002/2014RG000469.

Tkalčić, H., Romanowicz, B. & Houy, N., 2002. Constraints on D′′ structure using PKP (AB–DF), PKP (BC–DF) and PcP–P traveltime data from broad-band records, *Geophys. Res. Lett.,* **149**(3), 599–616.

Tkalčić, H., Bodin, T., Young, M. & Sambridge, M., 2013. On the nature of the P-wave velocity gradient in the inner core beneath Central America, *Journal of Earth Science,* **24**(5), 699–705.

Waszek, L. & Deuss, A., 2011. Distinct layering in the hemispherical seismic velocity structure of Earth's upper inner core, *J. geophys. Res.: Solid Earth (1978–2012),* **116**(B12), doi:10.1029/2011JB008650.

Waszek, L., Irving, J. & Deuss, A., 2011. Reconciling the hemispherical structure of Earth's inner core with its super-rotation, *Nature Geoscience,* **4**(4), 264–267.

Wen, L. & Niu, F., 2002. Seismic velocity and attenuation structures in the top of the Earth's inner core, *J. geophys. Res.: Solid Earth (1978–2012),* **107**(B11), ESE–2.

Wessel, P. & Smith, W.H.F., 1991. Free software helps map and display data, *EOS, Trans. Am. geophys. Un.,* **72,** 441–446.

Wessel, P. & Smith, W.H.F., 1998. New, improved version of the Generic Mapping Tools released, *EOS, Trans. Am. geophys. Un.,* **79,** 579.

Woodhouse, J.H., Giardini, D. & Li, X.-D., 1986. Evidence for inner core anisotropy from free oscillations, *Geophys. Res. Lett.,* **13**(13), 1549–1552.

Yoshida, S., Sumita, I. & Kumazawa, M., 1996. Growth model of the inner core coupled with the outer core dynamics and the resulting elastic anisotropy, *J. geophys. Res.: Solid Earth,* **101**(B12), 28 085–28 103.

Yu, W.-c. & Wen, L., 2006. Inner core attenuation anisotropy, *Earth planet. Sci. Lett.,* **245**(3), 581–594.